Determining the optimum migration aperture from traveltimes

C. Vanelle and D. Gajewski

email: *vanelle@dkrz.de*

keywords: *traveltimes, migration, true-amplitude, aperture*

ABSTRACT

True-amplitude migration based on a weighted diffraction stack is a task of high computational costs. These can be significantly reduced if the involved summation is carried out only over traces which really contribute to the stack result, i.e., a limited aperture instead of the whole aperture of the experiment. We introduce a technique to determine an optimum migration aperture that needs only traveltime tables as input information. These are also used for the "on the fly computation" of the true-amplitude weight functions and for an efficient and highly accurate traveltime interpolation. The new strategy leads to considerable savings in computational time and storage. A synthetic example illustrates the method.

INTRODUCTION

True-amplitude migration is a particular form of Kirchhoff-type migration. It is based on a weighted summation stack along diffraction time surfaces. If the summation is carried out over the whole aperture of the experiment, this becomes a very time consuming process, not only because of the summation itself, but also for the computation of proper weight functions. Although this latter problem can be overcome by determining weights from traveltimes directly (Vanelle and Gajewski, 2001c), the requirements in computational time are not the only difficulty: traces, where the diffraction time and the traveltime of the associated reflected event differ by more than the duration of the source pulse (this criterion defines the minimum migration aperture), do not contribute to the desired migration result. Including them in the summation leads to an increase in migration noise. Thus, a restriction to the minimum aperture as an optimized migration aperture can significantly enhance the image quality as well as the computational efficiency. Also, once the minimum aperture is determined, boundary effects can be recognized as such.

Although it is a different physical concept, the definition of the optimized (minimum) aperture bears a strong formal relationship to the (first) Fresnel zone, the intersection surface of the

Fresnel volume with the reflector surface. In 1992, Červený and Soares propose an algorithm for Fresnel volume ray tracing. They *"believe that Fresnel volume ray tracing will find [...] applications [...] in the inversion of seismic data in the near future"*. Hubral et al. (1993a) describe the Fresnel zone in paraxial approximation in terms of second-order derivative matrices of traveltimes. For the zero-offset situation the projection of this paraxial Fresnel zone onto the earth's surface is given in Hubral et al. (1993b). Schleicher et al. (1997) derive an expression for the projected Fresnel zone for arbitrary measurement configurations. They also introduce an expression for the size of the optimum migration aperture, which is again derived using the paraxial approximation. They further show that in this approximation both, projected Fresnel zone and optimum migration aperture, coincide.

Schleicher et al. (1997) compute the optimum migration aperture by means of dynamic ray tracing. We suggest to determine the optimum aperture from coarse-gridded traveltime tables. These traveltime tables are needed in any event for the diffraction stack. We apply a fast and accurate traveltime interpolation from the coarse input grid onto a fine migration grid to compute the stacking surface. At the same time we use the interpolation coefficients to compute migration weight functions and to determine the migration aperture. This strategy highly improves the computational efficiency of true-amplitude migration. Since only traveltime tables on coarse grids are required, the amount of storage is also considerably reduced.

METHOD

A diffraction stack of the form (Schleicher et al., 1993a)

$$V(M) = -\frac{1}{2\pi} \iint\limits_{A} \mathrm{d}\xi_1 \, \mathrm{d}\xi_2 \, W(\xi_1, \xi_2, M) \; \left. \frac{\partial U(\xi_1, \xi_2, t)}{\partial t} \right|_{\tau_D(\xi_1, \xi_2, M)} \tag{1}$$

yields a true-amplitude migrated trace for a 3-D medium if proper weight functions $W(\xi_1, \xi_2, M)$ are applied. In Equation (1), $V(M)$ represents the migration output at a selected depth image point M, A is the aperture of the experiment (assumed to provide sufficient illumination). Also, $\partial U(\xi_1, \xi_2, t)/\partial t$ is the time derivative of the input seismic trace in terms of its trace coordinates (ξ_1, ξ_2), which describe the source and receiver location according to the given configuration. That derivative is evaluated at the diffraction traveltime surface, $t = \tau_D(\xi_1, \xi_2, M)$, that corresponds to the fixed image point, M, and varying source and receiver locations described by (ξ_1, ξ_2), within the aperture A. Since it is required for all Kirchhoff migration methods, we assume that an *a priori* velocity model exists. As described in Schleicher et al. (1993a), the weight function, $W(\xi_1, \xi_2, M)$, can be expressed in terms of dynamical quantities that refer to the ray segments SM and GM, which connect the source at $S = S(\xi_1, \xi_2)$ and the receiver at $G = G(\xi_1, \xi_2)$. We use the weight function

$$W(\xi_1, \xi_2, M) = \frac{\sqrt{\cos\alpha_s \cos\alpha_g}}{v_s} \; \frac{\left| \det[\underline{\mathsf{N}}_1{}^{\top} \underline{\mathbf{\Sigma}} + \underline{\mathsf{N}}_2{}^{\top} \underline{\mathbf{\Gamma}}] \right|}{\sqrt{|\det \underline{\mathsf{N}}_1 \, \det \underline{\mathsf{N}}_2|}} \, \mathrm{e}^{-i\frac{\pi}{2}(\kappa_1 + \kappa_2)} \quad , \tag{2}$$

which is equivalent to the one derived by Schleicher et al. (1993a), but uses a different notation. In Equation (2), v_s is the velocity at the source. The angles α_s and α_g are the emergence angle at

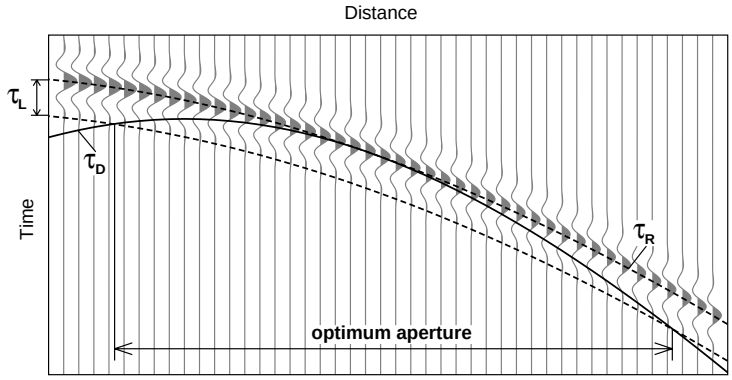

Figure 1: Schematic seismic section for a single reflector and traveltime curve for a diffraction point on the reflector. Dashed lines: reflection traveltime τ_R (coinciding with the events) and $\tau_R + \tau_L$. Solid line: diffraction traveltime τ_D. Traces outside the optimum aperture, which is given by the intersection points between the diffraction curve and the "end" of the signal, do not contribute to the diffraction stack.

the source and the incidence angle at the receiver. The matrices $\underline{\mathsf{N}}_1$ and $\underline{\mathsf{N}}_2$ contain second-order traveltime derivatives and are explained further below. The quantities κ_n are KMAH indices, where the index 1 in κ_n and $\underline{\mathsf{N}}_n$ refers to the ray segment SM, and index 2 to GM. The matrices $\underline{\Sigma}$ and $\underline{\Gamma}$ are configuration matrices associated with the trace coordinates, e.g., for a Common-Shot configuration $\underline{\Sigma} = \underline{0}$ (zero) and $\underline{\Gamma} = \underline{1}$ (the unit matrix). Please refer to Schleicher et al. (1993a) for details.

Depth migration using Equation (1) leads to high computational costs. For each subsurface point under consideration the diffraction time surface must be computed and for each combination of source-subsurface-receiver points the individual weight function is required. We have shown that the necessary amount of computational time and storage can be significantly reduced if migration weights are determined "on the fly" (i. e. not kept in the computer memory) from traveltimes (Vanelle and Gajewski, 2001c). These traveltimes need only be given on coarse grids and can at the same time be used as input data for an efficient interpolation onto the required fine migration grid (Vanelle and Gajewski, 2001b).

A further reduction of the computational effort is possible, if only those traces are summed up that really contribute to the stack (1). Figure 1 shows an extract of a seismic section for a single reflector and a diffraction traveltime curve for a point on the reflector. One can easily see that only those traces contribute to the stack where the diffraction traveltime curve τ_D is within the reflection traveltime τ_R and τ_R plus the duration of the signal, τ_L. Schleicher et al. (1997) use this criterion to define the minimum aperture which is also the optimum aperture:

$$|\tau_F| = |\tau_D - \tau_R| \leq \tau_L \quad , \tag{3}$$

where τ_F is the difference between diffraction and reflection traveltime.

To find an expression for the optimum aperture as it is given by Equation (3), we expand τ_F into a second-order Taylor series with respect to the 2-D source-receiver location coordinates $\xi = (\xi_1, \xi_2)$. The expansion is centered at the stationary point ξ^*, where $\tau_D = \tau_R$ and $\vec{\nabla}\tau_F = 0$:

$$\tau_F = \frac{1}{2}\,(\xi - \xi^*)^{\top} \underline{\mathsf{H}}_F\,(\xi - \xi^*) \quad , \tag{4}$$

in which $\underline{\mathsf{H}}_F$ is the Hessian matrix of the traveltime difference τ_F. With this equation and Equation (3), the optimum aperture in paraxial approximation is given by (Schleicher et al., 1997):

$$\frac{1}{2}\,|(\xi - \xi^*)^{\top} \underline{\mathsf{H}}_F (\xi - \xi^*)| = \tau_L \quad . \tag{5}$$

The matrix $\underline{\mathsf{H}}_F$ in Equation (5) can be written in terms of second-order spatial derivatives of traveltimes. To find an appropriate expression for $\underline{\mathsf{H}}_F$ we introduce specific 2-D Cartesian coordinate systems. These are located on the tangent planes to the recording surface at the source and the receiver, as well as on the tangent plane to the reflector at the reflection point. Details can be found in Vanelle and Gajewski (2001a). Using these coordinate systems, we split up reflection and diffraction traveltimes into the traveltime τ_1 of the ray segment from an initial source at $\mathbf{s}$ to the subsurface point at the position $\mathbf{r}$ (we denote this ray segment by the index 1), and the traveltime τ_2 from a receiver at the coordinate $\mathbf{g}$ to $\mathbf{r}$ (denoted by the index 2). The traveltimes τ_1 and τ_2 are in the paraxial approximation given by

$$\tau_n(\mathbf{x}_n, \mathbf{r}) = \tau_{0_n} + \mathbf{q}_{0_n}\,\Delta\mathbf{r} - \mathbf{p}_{0_n}\,\Delta\mathbf{x}_n - \Delta\mathbf{x}_n{}^{\top} \underline{\mathsf{N}}_n\,\Delta\mathbf{r} + \frac{1}{2}\,\Delta\mathbf{r}^{\top} \underline{\mathsf{G}}_n\,\Delta\mathbf{r} - \frac{1}{2}\,\Delta\mathbf{x}_n{}^{\top} \underline{\mathsf{S}}_n\,\Delta\mathbf{x}_n \quad , \tag{6}$$

where for n=1 the vector $\mathbf{x}_1$=**s**, and for n=2 the vector $\mathbf{x}_2$=**g**. The traveltime τ_{0_n} is $\tau(\mathbf{x}_{0_n}, \mathbf{r}_0)$. The slowness vectors $\mathbf{p}_{0_n}$ at $\mathbf{x}_{0_n}$ and $\mathbf{q}_{0_n}$ at $\mathbf{r}_0$ correspond to the first order derivatives (the index n for the considered ray branch is omitted in the following equations (7) and (8)):

$$p_{0_I} = -\left.\frac{\partial\tau}{\partial x_I}\right|_{\mathbf{x}_0,\mathbf{r}_0} \qquad q_{0_I} = \left.\frac{\partial\tau}{\partial r_I}\right|_{\mathbf{x}_0,\mathbf{r}_0} \quad . \tag{7}$$

The second order derivatives are given by the matrices $\underline{\mathsf{S}}_i$, $\underline{\mathsf{G}}_i$ and $\underline{\mathsf{N}}_i$ with

$$\begin{aligned} S_{IJ} &= -\left.\frac{\partial^2\tau}{\partial x_I \partial x_J}\right|_{\mathbf{x}_0,\mathbf{r}_0} = S_{JI} \\ G_{IJ} &= \left.\frac{\partial^2\tau}{\partial r_I \partial r_J}\right|_{\mathbf{x}_0,\mathbf{r}_0} = G_{JI} \\ N_{IJ} &= -\left.\frac{\partial^2\tau}{\partial x_I \partial r_J}\right|_{\mathbf{x}_0,\mathbf{r}_0} \neq N_{JI} \quad . \end{aligned} \tag{8}$$

Vectors and matrices have dimension two and represent a suitable projection onto the registration surface at $\mathbf{x}_{0_n}$, and the assumed reflector at $\mathbf{r}_0$. Suitable in this context means that the curvature of the registration surface and the reflector are also taken into consideration.

The matrices introduced in Equation (8) are ingredients of a propagator matrix that is used in *surface-to-surface* propagation (Schleicher et al., 1993b). One result of the application of the propagator formalism is the following expression for the matrix $\underline{\mathsf{H}}_F$:

$$\underline{\mathsf{H}}_F = \left(\underline{\mathsf{N}}_1{}^{\top}\underline{\Sigma} + \underline{\mathsf{N}}_2{}^{\top}\underline{\Gamma}\right)^{\top}\left(\underline{\mathsf{G}}_1 + \underline{\mathsf{G}}_2\right)^{-1}\left(\underline{\mathsf{N}}_1{}^{\top}\underline{\Sigma} + \underline{\mathsf{N}}_2{}^{\top}\underline{\Gamma}\right) \quad . \tag{9}$$

The matrix $\underline{\mathsf{H}}_F$, more precisely the matrices $\underline{\mathsf{G}}_n$ depend on the curvature of the reflector under consideration. Therefore, the determination of $\underline{\mathsf{H}}_F$ is possible for reflection points M, where the inclination and curvature of the reflector have been estimated from the *a priori* information, e.g., the velocity model or an image which results from a previous migration step. If the depth point M is such that these properties can not be determined, e.g., if no identified reflector surface exists, we may nevertheless consider it, because the migration described by Equation (1) yields non-negligible results only if the depth point M is on, or in the near vicinity of a reflector. Therefore we treat each depth point M, meaning each *candidate* for a reflection point as if it were a reflection point. It is in this sense that the term "reflector candidate" and the reflection traveltime τ_R are to be understood.

Schleicher et al. (1997) apply dynamic ray tracing for the computation of the second order derivative matrices that form $\underline{\mathsf{H}}_F$. We suggest to determine these matrices directly from the traveltimes that are in any event required for the diffraction time surface and the weight functions. As we will show in the following section, they can also be employed for an efficient traveltime interpolation onto the fine migration grid and to compute the true-amplitude weight functions.

IMPLEMENTATION

In this section we will explain how the migration weight functions and the optimum migration aperture are determined. Both can be expressed in terms of traveltime derivatives that are also used for traveltime interpolation. A three-dimensional variant of Equation (6) can be used for the traveltime interpolation. We have, however, shown, that a hyperbolic form of (6) yields higher accuracy than (6) (Vanelle and Gajewski, 2001b). Therefore we use a hyperbolic expansion of the traveltimes instead of (6). It is obtained by expanding τ^2 into a Taylor series of second order:

$$\tau^2(\hat{\mathbf{x}},\hat{\mathbf{r}}) = (\tau_0 + \hat{\mathbf{q}}_0\,\Delta\hat{\mathbf{r}} - \hat{\mathbf{p}}_0\,\Delta\hat{\mathbf{x}})^2 - 2\,\tau_0\Delta\hat{\mathbf{x}}^{\top}\underline{\hat{\mathsf{N}}}\,\Delta\hat{\mathbf{r}} + \tau_0\Delta\hat{\mathbf{r}}^{\top}\underline{\hat{\mathsf{G}}}\,\Delta\hat{\mathbf{r}} - \tau_0\Delta\hat{\mathbf{x}}^{\top}\underline{\hat{\mathsf{S}}}\,\Delta\hat{\mathbf{x}} \quad . \tag{10}$$

The vectors and matrices in this equation are not the same as in Equation (6) as they have dimension three (denoted by the hat) in an arbitrary Cartesian coordinate system. Since multi-fold traveltime tables are required for the stack anyway, we will use these to determine the coefficients of (10): Traveltimes for certain source-receiver combinations are inserted into (10). The resulting equations can then be solved for the slownesses and matrices. The procedure can be found in detail in Vanelle and Gajewski (2001b). Please note that Equation (10) also allows for the interpolation of sources, not only receivers.

The matrices $\underline{\mathsf{N}}_n$ and $\underline{\mathsf{G}}_n$ which are needed for the computation of $\underline{\mathsf{H}}_F$ (matrix $\underline{\mathsf{N}}_n$ is also needed for the weight functions) can be determined from $\underline{\hat{\mathsf{N}}}_n$ and $\underline{\hat{\mathsf{G}}}_n$ by rotating the latter onto

the tangent planes of the recording surface and the reflector candidate. Moreover, the curvature of the recording surface and the reflector has to be considered. The procedure is described in the Appendix. To do this, we assume that *a priori* information on the velocity model is available. For simple models the inclination of a reflector can be computed from the gradient of the velocity model. More generally, for example if the velocity model is smooth, it can be extracted from a previous migration. The determination of the reflector curvature follows similar lines. For image points that are not located on a reflector, this information will not be available. For these cases, however, the inclination and curvature are irrelevant, because the migration output will be negligible, regardless of inclination and curvature. For simplicity, we assume both to be zero for those points. If the reflector's inclination but not its curvature can be determined for a point which is located on the reflector, we expect that the approximation of the reflector by a locally plane surface will yield satisfactory results in many cases. This assumption appears to be acceptable since applicability of the ray method requires that the radius of reflector curvature is large compared to the wavelength. Moreover, the recovered reflection coefficient is a plane wave reflection coefficient.

The migration weight functions as well as the size of the optimum migration aperture can now be computed. We must, however, still determine the center of the aperture, that corresponds to the stationary ray. For this we can also use the coefficients of Equation (10), more precisely the slowness vectors. Again, we assume that the inclination angle of the reflector candidate be known and the slownesses are given accordingly. The incidence angle α_{inc} on the reflector is then given by

$$\cos\alpha_{\mathrm{inc}} = \sqrt{1 - v_{\mathrm{inc}}^2 \; \mathbf{q}_{0_1} \cdot \mathbf{q}_{0_1}} \quad , \tag{11}$$

where $\mathbf{q}_{0_1}$ is the (2-D) slowness vector at the candidate reflector of the ray from the source to the reflector. Similarly, $\mathbf{q}_{0_2}$ is the slowness vector of a ray from a geophone to the candidate reflector. The reflection angle α_{ref} is expressed by an equivalent of (11) but using $\mathbf{q}_{0_2}$ instead. Since the stationary ray obeys Snell's law, the center of the aperture is the geophone position where the difference between α_{inc} and α_{ref} is minimal.

EXAMPLE

We have applied our algorithm to simple generic models. These have the advantage of known analytic solutions for the involved quantities. Therefore they are very useful for the validation of the method. The example we give here is a two-layer model with an inclined interface. The inclination angle is 63° and the model has a velocity of 5km/s above and 6km/s below the reflector. A ray-synthetic common-shot section was computed using a Gabor wavelet with a signal length of 25ms. The migration was carried out first using the original noise-free data, and then for the same dataset with white (random) noise added, having a signal-to-noise ratio of 2. The noisy input section is shown in Figure 2. In both cases we have applied the optimum aperture as well as the complete aperture for comparison. In limiting the aperture we must, however, take into account that boxcar filtering produces undesirable effects like ringing or overshooting in the migrated image. Therefore a taper was applied at the endpoints of the aperture.

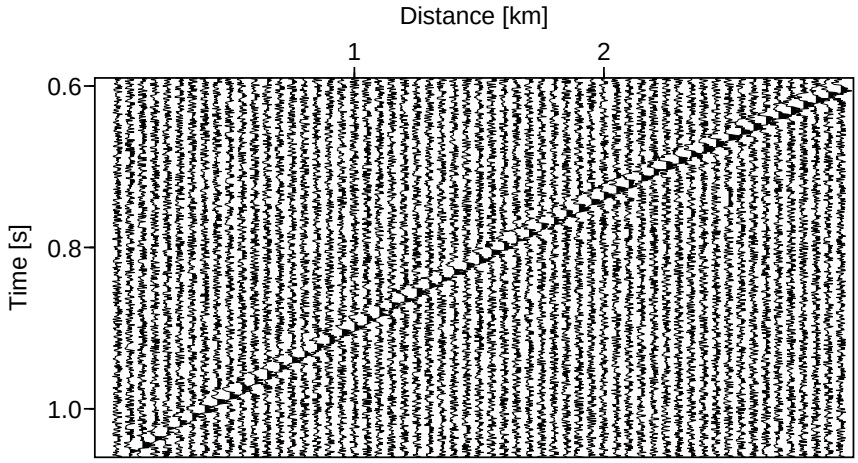

Figure 2: Synthetic common-shot section for a 63° inclined reflector: The receiver spacing is 10m but only every fifth trace is shown here. The signal-to-noise ratio is 2.

Figure 3 shows the recovered reflection coefficients from the noise-free section and analytic values. Compared to the whole aperture result, application of the optimum aperture leads to slightly overestimated reflection coefficients. This effect is more pronounced if the taper is omitted. For example, at 2.7 km distance the error of the recovered reflection coefficient is 1.3% if the whole aperture is used, it is 1.7% for the tapered optimum aperture and 3.0% for the optimum aperture without taper. The reason for the overestimation of the reflection coefficients is that the paraxial optimum aperture given by Equation (5) represents an approximation for the optimum aperture. Figure 4 demonstrates the difference between the exact optimum aperture (which can be computed for this type of model, but closed form solutions do not exist for arbitrary models) and the optimum aperture in paraxial approximation. Please observe in Figure 4 that traces within the required aperture, but not within the paraxial aperture would give negative contributions to the stack. This is why the reflection coefficients are overestimated. By applying the taper, additional traces outside of the paraxial aperture are allowed to contribute. This leads to a partial compensation of the overestimation caused by the errors of the paraxial aperture.

The AVO behavior, however, by which we signify the gradient or the general shape of the AVO is of more interest for interpretation than the absolute value of the reflection coefficients. It is less affected by the effect described above than the absolute value: Figure 3 shows that the AVO trend is preserved for all three cases, whether the whole aperture is used or the optimum aperture, with or without taper. For reflectors with moderate or no inclination the effect takes place on a smaller scale.

The reflection coefficients that result from the noisy input data on the 63° reflector are shown in Figure 5 together with the analytic values. Please keep in mind that in this example the quality of the input section is very poor. For a better signal-to-noise ratio the scatter in the recovered re-

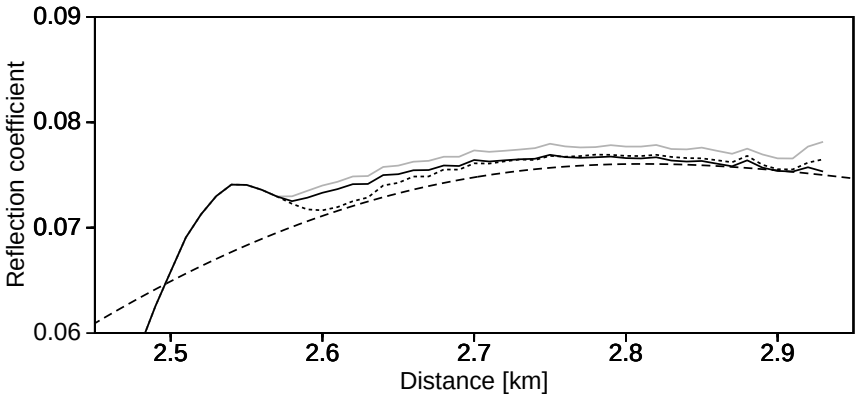

Figure 3: Recovered reflection coefficients from noise-free data for a 63° inclined reflector: Dashed line: analytic reflection coefficients. Dotted line: recovered coefficients if the whole aperture is used. Solid lines: recovered coefficients if the optimum aperture is used. The black line results from applying a taper to the aperture, the gray line follows without tapering. The reflection coefficients from the optimized aperture migration are overestimated (see text). The peak near 2.5km is a boundary effect caused by insufficient illumination of the reflector due to the limited extent of the receiver line.

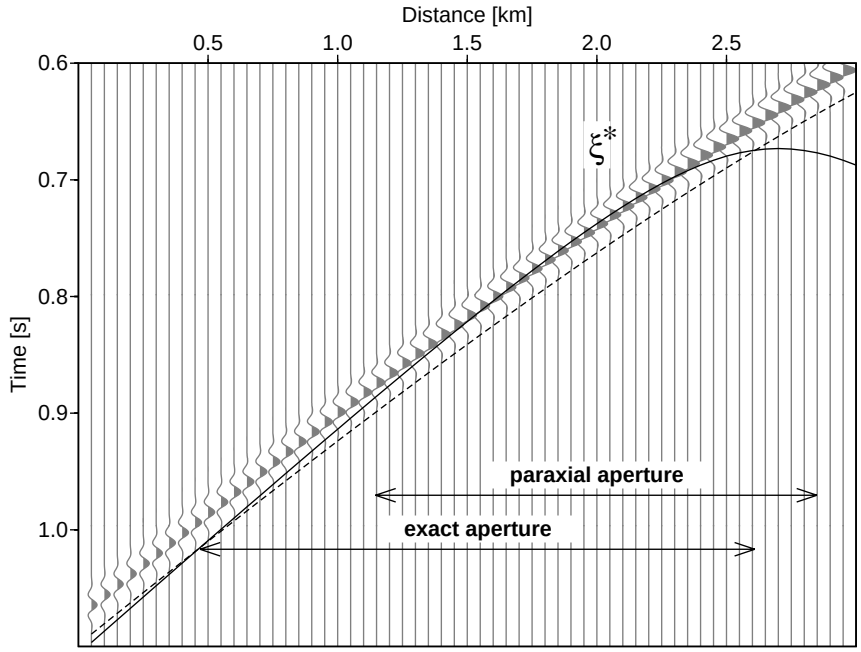

Figure 4: Exact and paraxial optimum migration aperture for a point on the 63° inclined reflector. Dashed line: reflection traveltime plus signal length $\tau_R + \tau_L$. Solid line: diffraction traveltime curve τ_D. The center of the paraxial aperture that corresponds to the stationary ray is located at ξ^*.

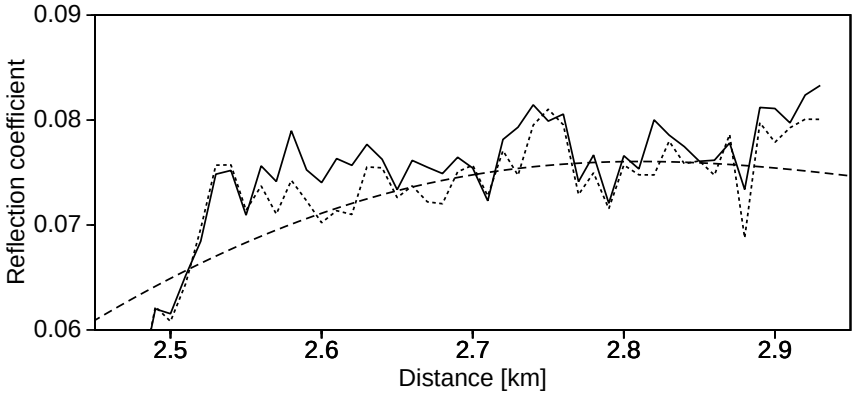

Figure 5: Results from noisy data for a 63° inclined reflector: Dashed line: analytic reflection coefficients. Solid line: recovered reflection coefficients if the optimum aperture is used. Dotted line: recovered coefficients if the whole aperture is used.

flection coefficients is significantly smaller. The migrated depth sections of the noisy data using the optimum aperture and the whole aperture are shown in Figure 6. In both cases the reflector has been migrated to the correct position but the image quality is improved if the optimum aperture is used. This effect may be more apparent if more than one arrival is present in the input section. If e.g., another reflection event in the data would cut through the one under consideration, it would add unwanted contributions to the stack, thus increasing the noise. By limiting the aperture, this higher noise can at least be averted for unwanted events that lie outside of the aperture.

We have shown that the application of our method to simple types of models yields good results in terms of image quality and recovered amplitude. The goal of our strategy is to provide these good results and at the same time reduce the requirements in computational time and storage. The storage problem can be overcome by using coarse gridded traveltimes as only input data. For example, a ratio of coarse grid spacing to fine grid spacing of ten leads to a factor of 10^{-5} less traveltime data that must be computed and held in storage. This high figure comes from the possibility of interpolating also sources, not only receivers.

The savings in computational time that result from the reduction of the migration aperture alone are difficult to estimate because of the various factors involved in the size of the required aperture. To give an idea about possible savings, we have compared the optimum aperture to the complete aperture for the case of a single, horizontal reflector. The results are shown for 2-D and 3-D in Figure 7. We have varied three parameters to demonstrate their influence on the aperture: the velocity in the upper part of the model, the reflector depth, and the signal length. For small cable lengths, the savings are moderate because the required apertures are not much smaller than the total cable length. If the cable length is increased, the ratio of required aperture to complete aperture decreases. The effect of the velocity and signal length are similar since both are closely related to the wavelength. For varying reflector depth we find a more pronounced change in

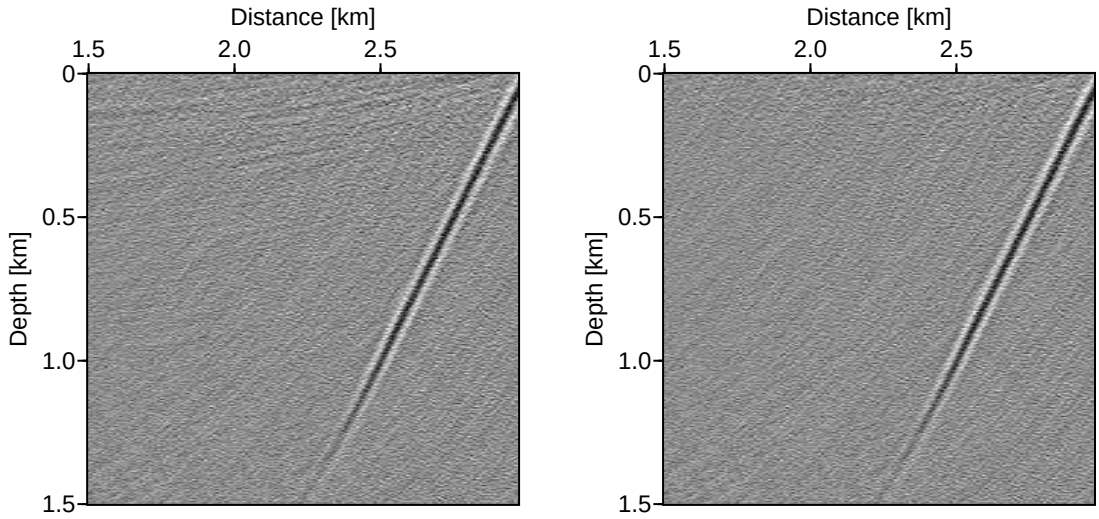

Figure 6: Migrated depth sections of noisy data for the 63° inclined reflector. Left: the whole aperture was used; right: only traces within the optimum aperture were used.

the behavior of the required aperture. The shallower the reflector is, the higher is the incidence angle of the wave with the normal to the registration surface, leading to an increase in apparent wavelength. This requires a larger aperture.

CONCLUSIONS

We have presented a new strategy for limited-aperture true-amplitude migration. Use of a limited aperture in migration can significantly reduce the computational time and at the same time enhance the image quality. The optimum migration aperture is determined from coarse gridded traveltime information only. These data are also the only input for the computation of migration weights, as well as for a fast and accurate traveltime interpolation onto the fine migration grid. The strategy of employing only coarse gridded traveltime data for the determination of all required quantities leads to considerable savings in computational time and, particularly, storage. A simple numerical example illustrates the applicability of the method and confirms the high potential savings in computational time.

PUBLICATIONS

The method of traveltime-based true-amplitude migration was introduced by Vanelle and Gajewski (2001c). More details on the traveltime interpolation and the determination of the coefficients can be found in Vanelle and Gajewski (2001c). In Vanelle and Gajewski (2001a) the authors describe how the optimum migration aperture can be obtained from traveltimes.

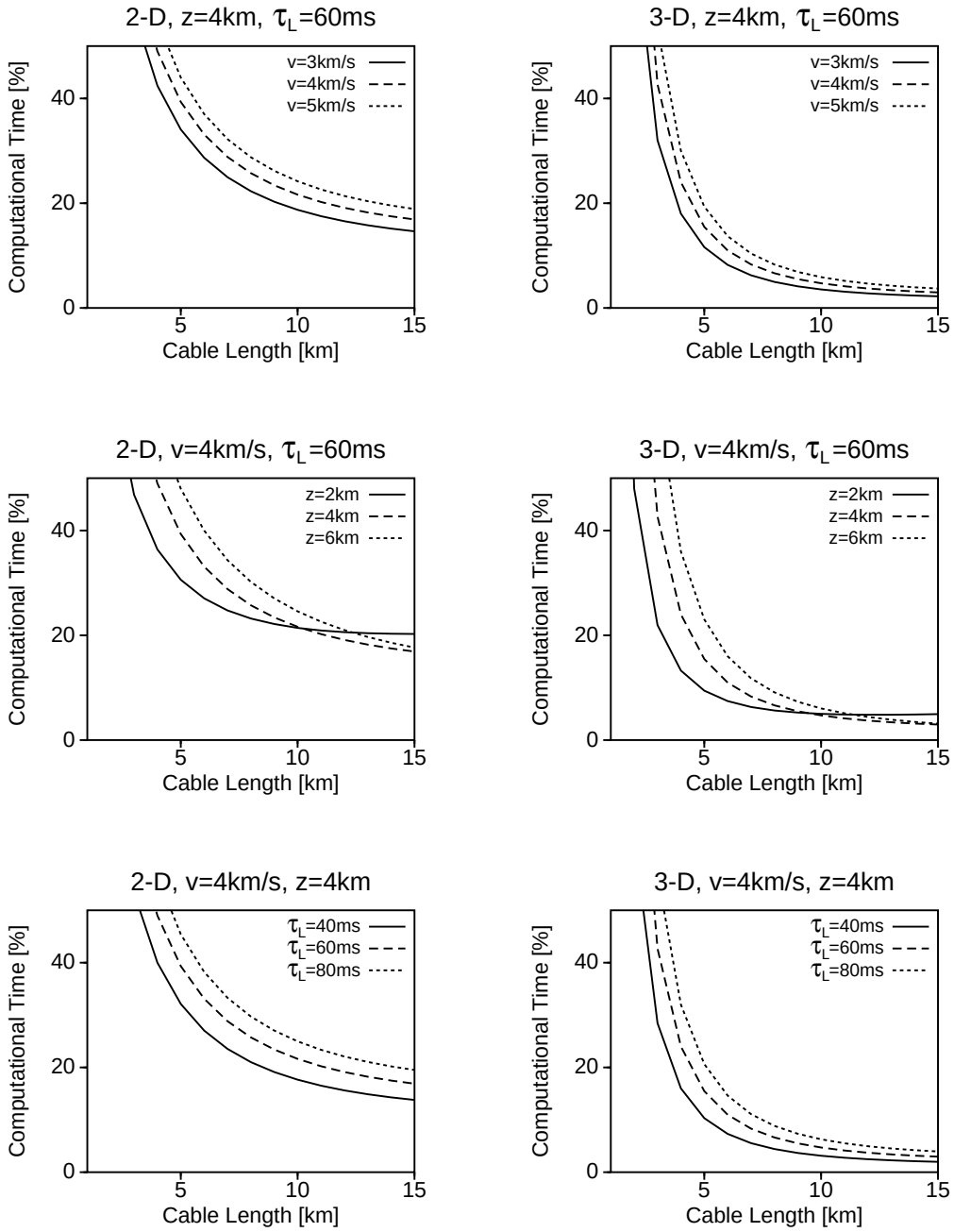

Figure 7: Possible savings in percent of computational time by using the optimum migration aperture (100% corresponds to the complete aperture). The velocity model considered here has a horizontal reflector between two layers of constant velocity. The parameters that were varied in these plots are the velocity in the upper layer (top), the reflector depth (middle) and the length of the source pulse (bottom), on the left for 2-D and right for 3-D.

ACKNOWLEDGMENTS

This work was partly supported by the German Research Society (DFG, Ga 350-10) and the sponsors of the Wave Inversion Technology (WIT) consortium. We would like to thank Martin Tygel, Kees Wapenaar, and Hugh D. Geiger for discussion. Suggestions from two anonymous reviewers considerably improved the paper. Continuous discussions with the members of the Applied Geophysics Group Hamburg are appreciated.

REFERENCES

Červený, V. and Soares, J. E. P. (1992). Fresnel volume ray tracing. *Geophysics*, 57:902–911.

Hubral, P., Schleicher, J., and Tygel, M. (1992). Three-dimensional paraxial ray properties, Part 1: Basic relations. *Journal of Seismic Exploration*, 1:265–279.

Hubral, P., Schleicher, J., and Tygel, M. (1993a). Three dimensional primary zero offset reflections. *Geophysics*, 58:692–702.

Hubral, P., Schleicher, J., Tygel, M., and Hanitzsch, C. (1993b). Determination of Fresnel zones from traveltime measurements. *Geophysics*, 58:703–712.

Schleicher, J., Hubral, P., Tygel, M., and Jaya, M. S. (1997). Minimum apertures and Fresnel zones in migration and demigration. *Geophysics*, 62:183–194.

Schleicher, J., Tygel, M., and Hubral, P. (1993a). 3D true-amplitude finite-offset migration. *Geophysics*, 58:1112–1126.

Schleicher, J., Tygel, M., and Hubral, P. (1993b). Parabolic and hyperbolic paraxial two-point traveltimes in 3D media. *Geophysics*, 41:495–513.

Vanelle, C. and Gajewski, D. (2001a). Determining the optimum migration aperture from traveltimes. *Journal of Seismic Exploration (in press)*.

Vanelle, C. and Gajewski, D. (2001b). Second-order interpolation of traveltimes. *Geophysical Prospecting (in press)*.

Vanelle, C. and Gajewski, D. (2001c). True amplitude migration weights from traveltimes. *Pure and Applied Geophysics (in press)*.

APPENDIX A

In this appendix we will explain how the second-order derivative matrices $\underline{\mathsf{N}}_n$ and $\underline{\mathsf{G}}_n$ are computed, if the surface under consideration is curved and its orientation does not coincide with the coordinate system in which the traveltime tables are given. In the traveltime system, denoted by a hat $\hat{}$, the parabolic 3-D traveltime expansion is given by

$$\tau(\hat{\mathbf{x}},\hat{\mathbf{r}}) = \tau_0 + \hat{\mathbf{q}}_0\,\triangle\hat{\mathbf{r}} - \hat{\mathbf{p}}_0\,\triangle\hat{\mathbf{x}} - \triangle\hat{\mathbf{x}}^{\top}\underline{\hat{\mathsf{N}}}\,\triangle\hat{\mathbf{r}} + \frac{1}{2}\,\triangle\hat{\mathbf{r}}^{\top}\underline{\hat{\mathsf{G}}}\,\triangle\hat{\mathbf{r}} - \frac{1}{2}\,\triangle\hat{\mathbf{x}}^{\top}\underline{\hat{\mathsf{S}}}\,\triangle\hat{\mathbf{x}} \quad . \tag{12}$$

In the coordinate system associated with the surfaces, e.g., the reflector, which we denote by a tilde˜, the traveltime expansion reads

$$\tau(\tilde{\mathbf{x}},\tilde{\mathbf{r}}) = \tau_0 + \tilde{\mathbf{q}}_0\,\Delta\tilde{\mathbf{r}} - \tilde{\mathbf{p}}_0\,\Delta\tilde{\mathbf{x}} - \Delta\tilde{\mathbf{x}}^\top \underline{\tilde{\mathsf{N}}}\,\Delta\tilde{\mathbf{r}} + \frac{1}{2}\,\Delta\tilde{\mathbf{r}}^\top \underline{\tilde{\mathsf{G}}}\,\Delta\tilde{\mathbf{r}} - \frac{1}{2}\,\Delta\tilde{\mathbf{x}}^\top \underline{\tilde{\mathsf{S}}}\,\Delta\tilde{\mathbf{x}} \quad . \tag{13}$$

The reflector coordinate system has the 1- and 2-axes in the reflector's tangent plane at $\tilde{\mathbf{r}}_0 = \hat{\mathbf{r}}_0$ and the 3-axis perpendicular to it. The vector $\Delta\tilde{\mathbf{r}} = (\Delta\mathbf{r},\Delta r_3)^\top = (\Delta r_1,\Delta r_2,\Delta r_3)^\top$ describes a point on the reflector. Its 3-component is given by

$$\Delta r_3 = \frac{1}{2}\,\Delta\mathbf{r}^\top \underline{\mathsf{F}}_r \Delta\mathbf{r} \quad , \tag{14}$$

where the 2×2 matrix $\underline{\mathsf{F}}_r$ is the curvature matrix of the reflector. It is zero for a plane reflector, therefore the 3-component vanishes in this case. The 2-D vector $\Delta\mathbf{r}$ is computed by

$$\Delta\mathbf{r} = \underline{1}_{2\times3}\,\hat{\underline{\mathsf{R}}}_r\,\Delta\hat{\mathbf{r}} \quad , \tag{15}$$

where the matrix $\underline{1}_{2\times3} = \underline{1}_{3\times2}^\top$ is

$$\underline{1}_{2\times3} = \begin{pmatrix} 1 & 0 & 0 \\ 0 & 1 & 0 \end{pmatrix} \quad . \tag{16}$$

The matrix $\hat{\underline{\mathsf{R}}}_r$ in Equation (15) describes the rotation into the tangent plane of the reflector. It is given by

$$\hat{\underline{\mathsf{R}}}_r = \begin{pmatrix} \cos\theta_r\cos\phi_r & -\cos\theta_r\sin\phi_r & \sin\theta_r \\ \sin\phi_r & \cos\phi_r & 0 \\ -\sin\theta_r\cos\phi_r & \sin\theta_r\sin\phi_r & \cos\theta_r \end{pmatrix} \quad . \tag{17}$$

(see Figure 8). Equations (14) and (17) also apply to the recording surface with the appropriate subscript x instead of r. The vectors $\Delta\mathbf{r}$ and $\Delta\mathbf{x}$ are the same as in Equation (6), the traveltime expansion into the reflector and recording surface.

Since the traveltime must not depend on the coordinate system, expressions (12) and (13) must be equal for a point on the reflector. Applying Equations (14) and (15) for both recording and reflector surface, and retaining only terms up to second order yields

$$\tau(\mathbf{x},\mathbf{r}) = \tau_0 + \mathbf{q}_0\,\Delta\mathbf{r} - \mathbf{p}_0\,\Delta\mathbf{x} - \Delta\mathbf{x}^\top \underline{\mathsf{N}}\,\Delta\mathbf{r} + \frac{1}{2}\,\Delta\mathbf{r}^\top \underline{\mathsf{G}}\,\Delta\mathbf{r} - \frac{1}{2}\,\Delta\mathbf{x}^\top \underline{\mathsf{S}}\,\Delta\mathbf{x} \quad . \tag{18}$$

The 2×2 matrices $\underline{\mathsf{N}}$, $\underline{\mathsf{G}}$, and $\underline{\mathsf{S}}$ are the same as in Equation (6) and are computed from the matrices $\hat{\underline{\mathsf{N}}}$, $\hat{\underline{\mathsf{G}}}$, and $\hat{\underline{\mathsf{S}}}$ as follows:

$$\begin{aligned} \underline{\mathsf{N}} &= \underline{1}_{2\times3}\,\hat{\underline{\mathsf{R}}}_x{}^\top \hat{\underline{\mathsf{N}}}\,\hat{\underline{\mathsf{R}}}_r\,\underline{1}_{3\times2} \quad , \\ \underline{\mathsf{S}} &= \underline{1}_{2\times3}\,\hat{\underline{\mathsf{R}}}_x{}^\top \hat{\underline{\mathsf{S}}}\,\hat{\underline{\mathsf{R}}}_x\,\underline{1}_{3\times2} + \frac{\cos\alpha_x}{v_x}\,\underline{\mathsf{F}}_x \quad , \\ \underline{\mathsf{G}} &= \underline{1}_{2\times3}\,\hat{\underline{\mathsf{R}}}_r{}^\top \hat{\underline{\mathsf{G}}}\,\hat{\underline{\mathsf{R}}}_r\,\underline{1}_{3\times2} + \frac{\cos\alpha_{\text{inc}}}{v_r}\,\underline{\mathsf{F}}_r \quad . \end{aligned} \tag{19}$$

The angle α_{inc} is the incidence angle on the reflector and α_x is the angle between the ray and the recording surface. The quantity $\cos\alpha_{\text{inc}}/v_r$ is the 3-component of the slowness vector in the reflector coordinate system (accordingly for $\cos\alpha_x/v_x$). Similar results were also derived by Hubral et al. (1992) using a different notation.

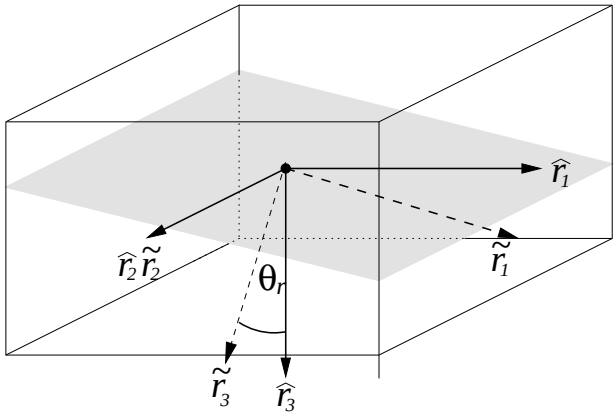

Figure 8: Rotation of 3-D second-order derivative matrices into the reflector tangent plane: the coordinate system of the reflector (gray) is denoted by a tilde $\tilde{}$. The Cartesian system that coincides with the system in which the traveltime tables are given is indicated by a hat $\hat{}$. The angle θ_r is the angle between the 3-axes in both systems. In this plot the angle ϕ_r is zero, as well as the curvature of the reflector.